Milestone 5 Final Report: Hybrid Lyot and Shaped Pupil Broadband Contrast Testbed Demonstration for WFIRST-AFTA

Eric Cady[a], Byoung-Joon Seo[a], Bala Balasubramanian[a], Frank Greer[a], Brian Gordon[a], N. Jeremy Kasdin[b], Brian Kern[a], Andy Kuhnert[a], David Marx[a], Camilo Mejia Prada[a], Dwight Moody[a], Richard Muller[a], Ilya Poberezhskiy[a], A.J. Riggs[b], John Trauger[a], Daniel Wilson[a], Victor White[a], Karl Yee[a], Neil Zimmerman[c], and Hanying Zhou[a]

[a] Jet Propulsion Laboratory, California Institute of Technology, Pasadena, CA. 91109

[b] Princeton University, Princeton, NJ 08544

[c] Space Telescope Science Institute, Baltimore, MD 21218

Contents

Copyright 2015. All rights reserved.

1 Overview

As laid out in original definitions to National Aeronautics and Space Administration (NASA) Headquarters and the Technical Analysis Committee (TAC), WFIRST-AFTA Coronagraphic Instrument (CGI) Milestone 5 was defined as:

> *The Occulting Mask Coronagraph (OMC) — Hybrid Lyot Coronagraph (HLC) or Shape Pupil Coronagraph (SPC) —in the High Constrast Imaging Testbed (HCIT) demonstrates* 10^{-8} *raw contrast with broadband light* (10%) *at* $550\,\mathrm{nm}$ *in a static environment.*

In this report, we will present repeated convergence below 9×10^{-9} mean contrast in the HCIT achieved by both HLC and SPC modes of the OMC, across a $3\,\lambda/D$ and $9\,\lambda/D$ dark hole in 10% broadband light centered at $550\,\mathrm{nm}$. These results were presented to the TAC on September 29th, 2015, concurrently with the results of WFIRST-AFTA CGI Milestone 6.

This report is structured as follows. Sec. 2 will briefly overview the technical background behind the SPC and HLC and provide the appropriate references. In Sec. 3, we highlight the configuration changes made for Milestone 5 from the previous milestones, since most of the testbed configuration has been covered already in previous milestone reports[1,2] and in peer-reviewed publications.[3–5] Data and analysis, including the contrast results, are presented in Sec. 4, while conclusions and future work are described in Sec. 5.

2 Technical Background

As the light from the WFIRST-AFTA telescope is delivered to the coronagraph instrument, the first pupil is formed at the Fast Steering Mirror (FSM) that corrects the Line of Sight (LoS) pointing jitter and drift using information from the Low Order Wavefront Sensing and Control (LOWFS/C) subsystem. The light is then delivered to two Deformable Mirrors (DMs), which perform active wavefront control to compensate for phase and amplitude imperfections in the optical train.

SPC and HLC are the two interchangeable coronagraph modes of the OMC operation. Shaped pupil masks use optimization to design a binary-valued pupil stop whose Point Spread Function (PSF) has regions of very high contrast; an occulting focal-plane mask then blocks the entirety of the PSF except these "dark holes". A coronagraph of this type was used for WFIRST-AFTA CGI Milestone 2; see [6] for more details of the design process and [3] for Milestone 2 configuration.

Hybrid Lyot Coronagraphs (HLCs), on the other hand, do not require a pupil stop; they use a joint optimization between the settings of two DMs, the complex transmission profile of a focal-plane mask, and the shape of a following Lyot stop to produce an intricate DM initial condition which provides broadband wavefront control and minimizes the effect of jitter. See [5, 7] for more details of the HLC design process.

3 Testbed Configuration, Operation, and Algorithm

Although SPC and HLC are planned to operate in a single testbed for Milestone 9, two separate testbeds were used for Milestone 5. The two testbeds used for SPC and HLC are essentially the same ones as used for Milestone 2 and 4, respectively. The Milestone 2 and 4 were intended for the narrowband contrast demonstration while Milestone 5 is for the broadband contrast demonstration. The majority of testbed configuration was retained, but several modification were necessary.

In this section, we hightlight crucial testbed modifications made for Milestone 5.

3.1 Configuration update in SPC testbed

Following testbed modificaitons have been made for Milestone 5 from Milestone 2 in SPC.

- The shaped pupil of Milestone 5 uses a 2nd generation design called Shape Pupil Lyot Coronagraph (SPLC), which augments the binary pupil plane mask and wedge-shaped occulting mask ("bowtie mask") of Milestone 2 with a 10%-undersized Lyot stop, which permits a smaller inner working angle than the pupil and bowtie alone. The DMs are nominally flat at the start of a wavefront correction sequence. Fig. 1 shows the masks used in the Milestone 5 work.

  As in Milestone 2, the shaped pupil mask is fabricated on a thick silicon wafer and used in reflection, with a reflective aluminum coating providing the "open" regions of the mask and black silicon processing[8] providing a highly-absorbing surface to act as the obscuration. While the optimized shape has changed in the past year, the underlying technology has not.

  The bowtie and the Lyot stop are both manufactured by etching holes through thinner silicon-on-insulator (SOI) wafers, creating shaped apertures with no underlying substrate in the open regions. One major change for Milestone 5 has been the reduction of the inner and outer working angles of the bowtie mask; the mask itself extends from 2.5-9 λ/D. However, the presence of the Lyot stop means the effective working region runs from 2.8-8.8 λ/D. The opening of the bowtie is increased to 65 degree.

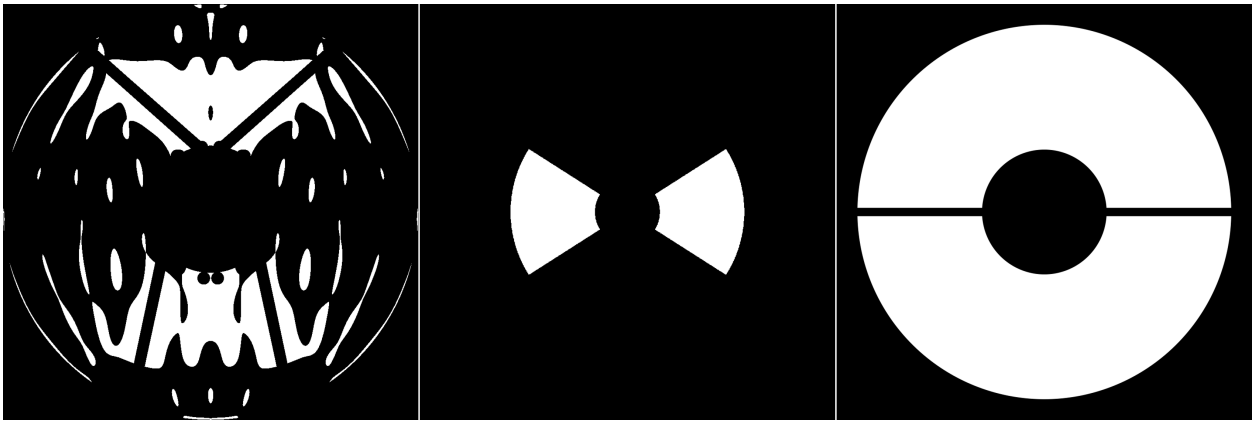

Fig 1 The three masks of a shaped pupil Lyot coronagraph. *Left.* Shaped pupil. *Center.* Bowtie focal plane mask. *Right.* Lyot stop.

- A second DM was introduced 1m downstream of the first DM, replacing the flat that was there previously. The introduction of a DM here had been part of the plan since the construction of the testbed. The first DM is same as in Milestone 2, the 64×64-actuator DM near the pupil. The presence of a second DM permitted the correction of phase and amplitude on both sides of the PSF simultaneously. This DM was 32×32, and necessitated a smaller system pupil than the one used previously.

- The Lyot stop was inserted on a 3-axis stage in a pupil plane downstream of the fifth off-axis parabola (OAP). The original design for the testbed had *not* included a Lyot stop, and the fit turned out to be rather tight, but achievable.

- One software change was the introduction of a focal plane mask tracking loop, as the centration requirements were tightened by the use of the bowtie as an active part of the correction, rather than just as a field stop as in Milestone 2. Pairs of speckles are created with sine waves on the DM, and sized to fall at the edge of the bowtie; the bowtie can then be adjusted in x and y to balance leakage.

3.2 Configuration update in HLC testbed

Following testbed modificaitons have been made for Milestone 5 from Milestone 4 in HLC.

- Unlike other coronagraphs such as the SPC, the DM shapes are one of the major design building blocks for the WFIRST-AFTA HLC.[7,9] That is, the DM facesheets have to be shaped properly to create a dark hole in conjunction with the hybrid occulter and the Lyot stop. The correct application of the designed DM shape to the testbed is crucial not only for acheiving a broadband dark hole but also for reducing the jitter sensitivity. Therefore, it is also refered to as "Jitter Insensitive Broadband DM solution". The designed DM shapes used in Milestone 5 are shown in Fig. 2. The required DM stroke has been considered with greater weight in the optimization process, requiring less than 163 nmPV−Surface and 184 nmPV−Surface for

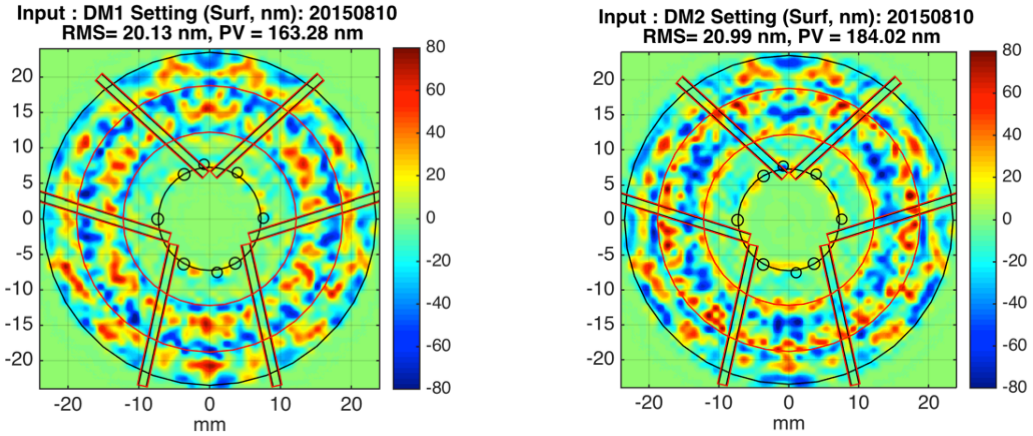

(a) DM1 design facesheet profile (b) DM2 design facesheet profile

Fig 2 "Jitter Insensitive Broadband DM solution" used in Milestone 5. This model-generated DM facesheet profile is applied to testbed before WFC to acheive a broadband dark hole.

DM1 and DM2, respectively. This represents $\sim 40\,\%$ decrease compared to previous HLC design iterations and is a positive developement as it increases the DM stroke range margin.

- The occulter is tilted by 15 degree with respect to the chief ray as shown in Fig. 3(a) while 9 degree was used in Milestone 4. Although the DM solution improves the chromaticity and reduces the jitter sensitivity, it introduces an energy increase of the outer PSF. This increases the occulter ghost impact, compared to Milestone 4 narrowband DM settings. In order to reduce the occulter ghost, occulter tilt angle of 15 degree is used. Based on (a) occulter configuration information and (b) the outer PSF measurement with the field stop out as shown in Fig. 3, the ghost contribution to the dark hole is estimated as 2×10^{-9} at 550 nm, which agrees with measurement of umodulated light in the dark hole at 550 nm.

3.3 Configuration update in both testbeds

Following are the key modifications made for Milestone 5 in both testbeds.

- High power broadband laser source (EXB-6, NKT Photonics) was used for the broadband operation in conjuction with selectable bandpass filters.

- The software and algorithms continue to use standard HCIT practice: estimation is done with a series of "probes"; carefully chosen DM settings which modulate the electric field in the dark hole. Pairs of these may be used in conjunction with a model of the testbed to back out the complex electric field.[10] Correction is done with Electric Field Conjugation (EFC), an iterative algorithm for minimizing the electric field using a model of the effects of each actuator poke.[11]

  While a single monochromatic band was used in the previous Milestones, both testbeds, in Milestones 5, use five 2% bands over 10% spectrum for broadband sensing and control. We sense the complex electric field in the dark hole using five bands and control all bands simultaneously to achieve the best possible 10% broadband DM solution.

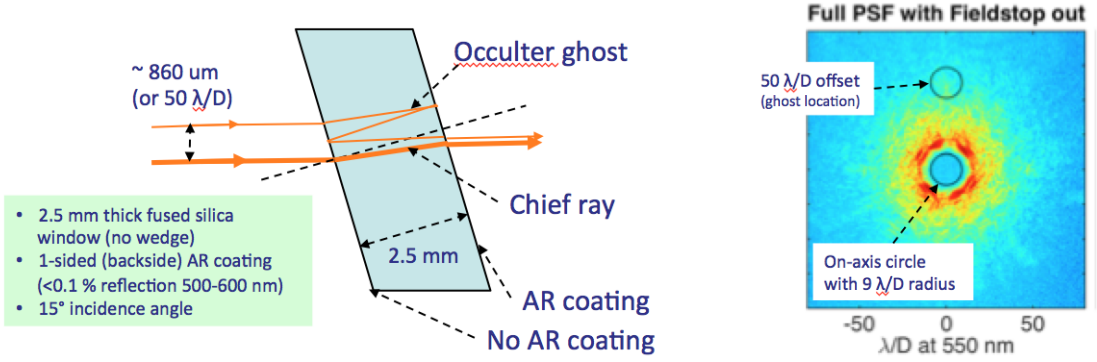

(a) (b)

Fig 3 (a) Occulter configuration and occulter ghost optical path, (b) the outer PSF used for occulter ghost estimation. The outer PSF is normally blocked from the camera by an annular field stop.

4 Data and analysis

4.1 SPC Result

For the SPC Milestone 5 data collection, three runs were done on three days, in each case simultaneously controlling over 5 2% bands spanning $522.5 - 577.5$nm (10%-band around 550nm). The region of interest was a 65° wedge running from $2.8 - 8.8\lambda/D$. The residuals are subsequently corrected for the effects of off-axis coronagraph throughput; in a shaped pupil Lyot coronagraph, this primarily causes the "starlight" to be suppressed less effectively near the edges of the bowtie. Figure 4 shows the per-pixel multiplier; the measured intensity is derated by up to a factor of two near the edges of the working region.

The testbed was exposure-time limited; each iteration took approximately 45 minutes. To mitigate the overhead associated with long iteration sequences while demonstrating repeatability, we set the DM to a neutral flat setting and then to a DM setting associated with a previous broadband dark hole. We ran several iterations on three of the five bands—the first, middle and last—with an oversized dark hole to attenuate bright wing speckles which can leak into the dark hole, and then correction in all five bands over a region matched to the bowtie opening. Figure 5 shows the normalized intensities over this last 5-band portion of the iteration sequence, and Figure 6 gives the final contrasts after off-axis correction and the associated images planes. All three runs had a contrast less than 8.8×10^{-9}. Contrast error due to photometric calibration is less than 2%.

The SPLC had been designed to work in an 18% band centered around 550nm, and two runs were done in 14% and 18% bands, producing contrasts of 9.6×10^{-9} and and 1.6×10^{-8}. (See Fig. 7.) In both cases, contrast was dominated by the outermost spectral bands.

4.2 HLC Result

Fig. 8(a) shows one of the raw high contrast images achieved in the HLC testbed. The averaged raw contrast is 8.54×10^{-9} across the full 360 degrees region between $3\,\lambda$/D and $9\,\lambda$/D in 10% broadband light centered at 550 nm. Two yellow circles in Fig. 8(a) are drawn to represent the $3\,\lambda$/D and $10\,\lambda$/D radius field of view. This dark hole is obtained by averaging the five 2% band dark

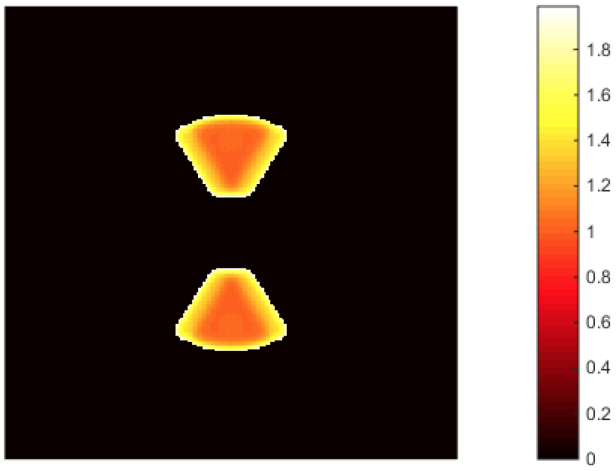

Fig 4 Per-pixel correction factor which multiplies the measured intensity to correct for the off-axis throughput of a planet, which is reduced when the planet falls near the edge of the bowtie.

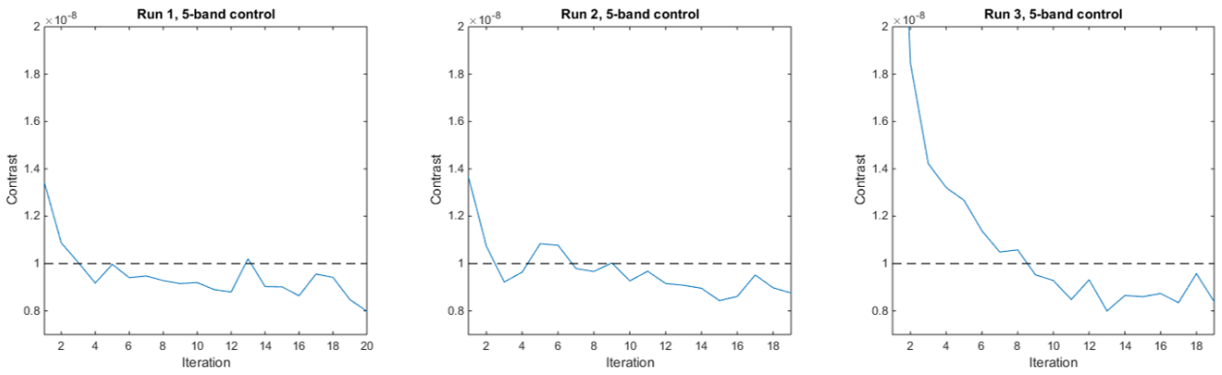

Fig 5 Normalized intensity per iteration during the 5-band correction for the each of the three milestone runs.

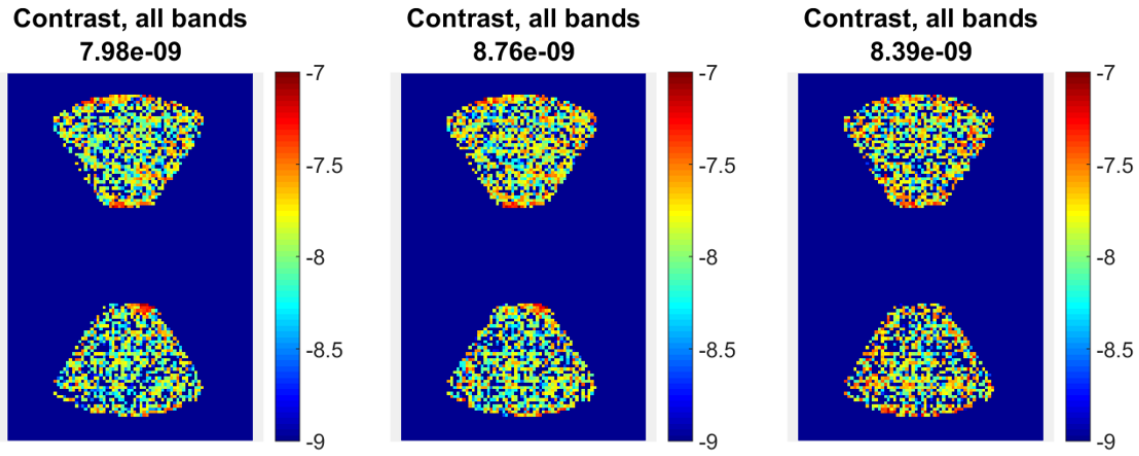

Fig 6 Image-plane contrast distributions in the final iteration of each SPC milestone run.

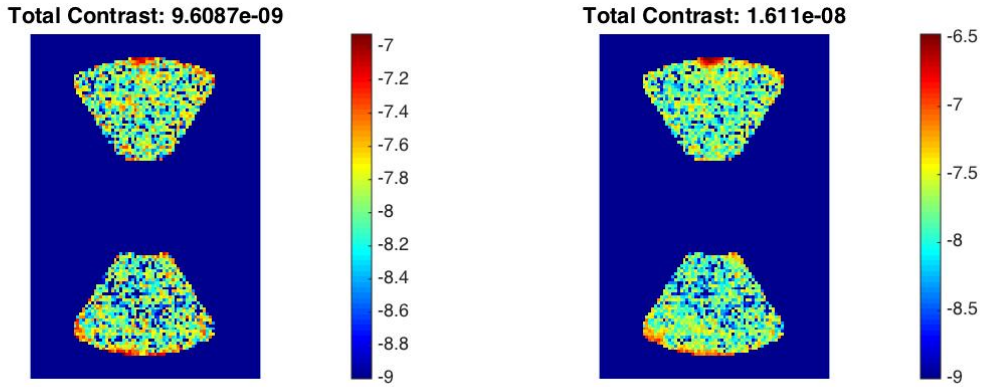

(a) (b)

Fig 7 *Left:* Image-plane after correction in a 14% band around 550nm. *Right:* Image-plane after correction in a 18% band around 550nm.

holes, whose center wavelengths are 530 nm, 540 nm, 550 nm, 560 nm, and 570 nm, respectively. The contrast is measured with an arbitrary polarization with no polarizer in the optical train.

In this particular case, we use the same occulter used for the milestone 4 with a larger tilt angle of 15 degree. The contrast error is estimated to be less than 2 % due to photometry estimation uncertainty.

Achieved contrast performance is consistent and predictable as we can obtain repeated convergence below 9×10^{-9} average contrast. Three independent WFC runs are demonstrated in Fig. 9. In each run, we start WFC from a testbed-generated DM solution, which is the first DM solution after iterations in testbed starting from the DM solution as described in Sec. 3. Getting the testbed-generated DM solution from the DM solution may require more iterations due the possible discrepancy between the model and the actual testbed as discussed in [2]. However, once we obtain a testbed-generated DM solution, we achieve the dark hole contrast exceeding 1×10^{-8} in fewer

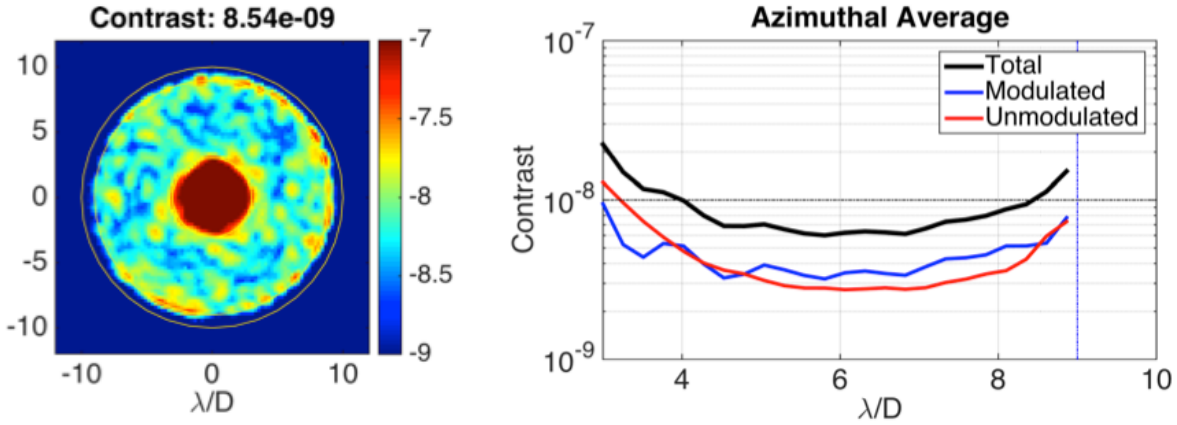

(a) (b)

Fig 8 Averaged raw contrast of 8.54×10^{-9} is obtained in this example considering the full 360 degrees region between 3 λ/D and 9 λ/D. The raw contrast used here is explicitly defined by Krist, et. al.[12] (a) 2D contrast image, (b) its azimuthal average. The black, blue, and red curves in Fig. 8(b) (and Fig. 9) denote the total, modulated, and unmodulated light components, respectively. See [2] for definition of modulated and unmodulated light.

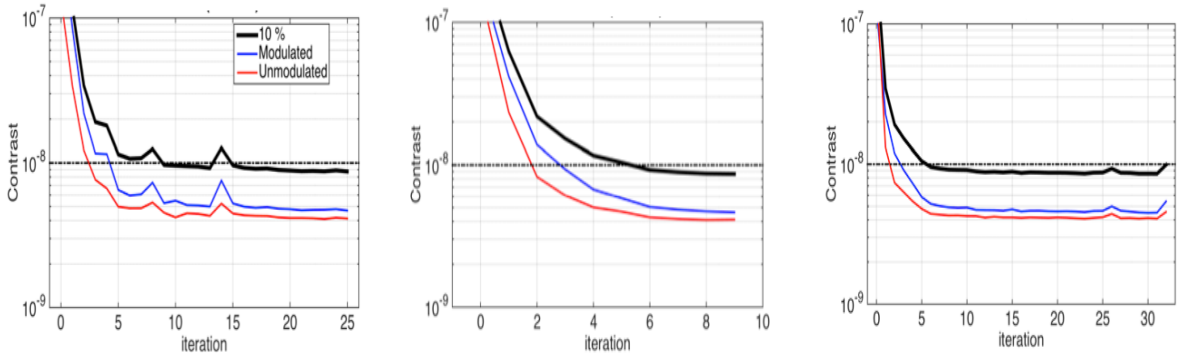

(a) (b) (c)

Fig 9 Mean contrast across the dark hole as a function of WFC iteration number, for each of the three runs. The black, blue, and red curves denote the total, modulated, and unmodulated residual star light, respectively.

than 10 iteration cycles for every run, as shown in Fig. 9. The iteration period is approximately 15 minutes.

5 Conclusion and Future Work

The next step in the OMC technology maturation plan is Milestone 9, which is the starlight suppression demonstration in presence of simulated input wavefront disturbances expected on-orbit by the WFIRST-AFTA observatory. For this, a new OMC testbed has been designed, built and aligned. This testbed, analogously to the OMC flight instrument architecture, can be operated in two different modes: HLC and SPC. In the new dynamic OMC testbed, the AFTA Optical Telescope Assembly Simulator (OTA-S) serves as the front end. OTA-S has been built and demonstrated for Milestone 6 and is a sophisticated piece of ground support equipment designed to introduce line-of-site and other low order wavefront perturbations expected on-orbit on relevant timescales. The OMC will be presented with realistic dynamic input wavefront from the OTA-S and will rely on its LOWFS/C subsystem to sense and correct the dynamic wavefront down to the level that permits the WFIRST OMC to meet its science goals. Thus, the Milestone 9 will serve as an integrated and complete demonstration of the capabilities first shown for Milestones 5 and 6 on three separate testbeds. Milestone 9 is due in late 2016.

6 Acronyms

CGI Coronagraphic Instrument . . . 2
DM Deformable Mirror . . . 2
EFC Electric Field Conjugation . . . 5
FSM Fast Steering Mirror . . . 2
HCIT High Constrast Imaging Testbed . . . 2
HLC Hybrid Lyot Coronagraph . . . 1
LOWFS/C Low Order Wavefront Sensing and Control . . . 2
LoS Line of Sight . . . 2
NASA National Aeronautics and Space Administration . . . 2
OMC Occulting Mask Coronagraph . . . 2
PSF Point Spread Function . . . 2
SPC Shape Pupil Coronagraph . . . 1
SPLC Shape Pupil Lyot Coronagraph . . . 3
TAC Technical Analysis Committee . . . 2
WFC Wavefront Control

Acknowledgments

Presented WFIRST-AFTA coronagraph technology development work was carried out at the Jet Propulsion Laboratory using funding from NASA SMD and STMD. We acknowledge X. An, R. Diaz, D. Palmer, K. Patterson, D. Ryan, F. Shi, R. Zimmer and H. Tang for their contribution to testbed layout, assembly, and alignment, J. Krist for modeling advice, F. Greer, K. Balasubramanian, V. White, and R. Calvet for device fabrication, S. Macenka, and F. Zhao for programmatic advice.

References

1 E. Cady, X. An, B. Balasubramanian, R. Diaz, J. Kasdin, B. Kern, A. Kuhnert, B. Nemati, K. Patterson, I. Poberezhskiy, A. Riggs, D. Ryan, H. Zhou, and R. Z. N. Zimmerman, "Milestone 2 final report: Shaped pupil narrowband contrast," *JPL Document* , 2014.

2 B.-J. Seo, B. Gordon, B. Kern, A. Kuhnert, D. Moody, R. Muller, I. Poberezhskiy, J. Trauger, and D. Wilson, "Milestone 4 Final Report: Narrowband Contrast Testbed Demonstration of Hybrid Lyot Coronagraph for WFIRST-AFTA," *JPL Document* , 2014.

3 E. Cady, C. Mejia Prada, X. An, K. Balasubramanian, R. Diaz, N. J. Kasdin, B. Kern, A. Kuhnert, B. Nemati, I. Poberezhskiy, A. J. E. Riggs, R. Zimmer, and N. Zimmerman, "Demonstration of high contrast with an obscured aperture with the wfirst-afta shaped pupil coronagraph," *Journal of Astronomical Telescopes, Instruments, and Systems Special Section, SPIE* **2**(1), p. 011004, 2015.

4 B.-J. Seo, B. Gordon, B. Kern, A. Kuhnert, D. Moody, R. Muller, I. Poberezhskiy, J. Trauger, and D. Wilson, "Hybrid Lyot Coronagraph for WFIRST-AFTA: Occulter Fabrication and High Contrast Narrowband Testbed Demonstration," *Journal of Astronomical Telescopes, Instruments, and Systems Special Section, SPIE* , 2015.

5 J. Trauger, B. Gordon, J. Krist, and D. Moody., "Hybrid Lyot Coronagraph for WFIRST-AFTA: coronagraph design and performance metrics (To be published)," *Journal of Astronomical Telescopes, Instruments, and Systems Special Section, SPIE* , 2015.

6 N. Zimmerman, A. J. E. Riggs, N. J. Kasdin, A. Carlotti, and R. Vanderbei, "Shaped pupil lyot coronagraphs: High-contrast solutions for restricted focal planes," *Accepted by* JATIS , 2015.

7 J. Trauger, D. Moody, and B. Gordon, "Complex apodized Lyot coronagraph for exoplanet imaging with partially obscured telescope apertures," 2013.

8 K. Balasubramanian, V. White, K. Yee, P. Echternach, R. Muller, M. Dickie, E. Cady, C. M. Prada, D. Ryan, I. Poberezhskiy, B. Kern, H. Zhou, J. Krist, B. Nemati, A. J. Eldorado Riggs, N. T. Zimmerman, and N. J. Kasdin, "WFIRST-AFTA coronagraph shaped pupil masks: design, fabrication, and characterization," *Journal of Astronomical Telescopes, Instruments, and Systems* **2**(1), p. 011005, 2015.

9 J. Trauger, D. Moody, B. Gordon, J. Krist, and D. Mawet, "A hybrid lyot coronagraph for the direct imaging and spectroscopy of exoplanet systems: recent results and prospects," 2011.

10 A. Give'on, B. D. Kern, and S. Shaklan, "Pair-wise, deformable mirror, image plane-based diversity electric field estimation for high contrast coronagraphy," in *Society of Photo-Optical Instrumentation Engineers (SPIE) Conference Series*, *Society of Photo-Optical Instrumentation Engineers (SPIE) Conference Series* **8151**, Sept. 2011.

11 A. Give'on, "A unified formalism for high contrast imaging correction algorithms," *Techniques and Instrumentation for Detection of Exoplanets IV* **7440**, p. 74400D, SPIE, 2009.

12 J. Krist, B. Nemati, and B. Mennesson, "Numerical modelling of the proposed WFIRST-AFTA coronagraphs and their predicted performances," *Journal of Astronomical Telescopes, Instruments, and Systems Special Section, SPIE* , 2015.